STIS Echelle Observations of the Intrinsic UV Absorption in the Seyfert 1 Galaxy NGC 3783.

S. B. Kraemer[2], D. M. Crenshaw[2], & J.R Gabel[2]

Received —————————; accepted —————————

[2]Catholic University of America, NASA's Goddard Space Flight Center, Code 681, Greenbelt, MD 20771; stiskraemer@yancey.gsfc.nasa.gov, crenshaw@buckeye.gsfc.nasa.gov, gabel@iacs.gsfc.nasa.gov.

ABSTRACT

We present observations of the UV absorption lines in the Seyfert 1 galaxy NGC 3783, obtained with the medium resolution ($\lambda/\Delta\lambda \approx 40,000$) echelle gratings of the Space Telescope Imaging Spectrograph (STIS) on the *Hubble Space Telescope (HST)*. The spectra reveal the presence of three kinematic components of absorption in Lyα, C IV, and N V, at radial velocities of -1365, -548, and -724 km s^{-1} with respect to the systemic velocity of the host galaxy (Components 1, 2 and 3, respectively); Component 1 also shows absorption by Si IV. Component 3 was not detected in any of the earlier Goddard High Resolution Spectrograph (GHRS) spectra, and the C IV absorption in the other components has changed since the most recent GHRS observation obtained $\sim$ 5 yr earlier. Somewhat unexpectedly, each component has a covering factor (of the continuum source + broad emission line region) of ~ 0.6. We have calculated photoionization models to match the UV column densities in each of the three components. The models predict a zone characterized by high ionization parameter (U = 0.65 – 0.80) and column density (6.4 x 10^{20} – 1.5 x 10^{21} cm^{-2}) for each component, and a second, low ionization (U = 0.0018) and low column density (4.9 x 10^{18} cm^{-2}) zone for Component 1. Based on the model results, there should be strong absorption in the bandpass of the *Far Ultraviolet Spectroscopic Explorer (FUSE)*, 912 Å – 1200 Å , including saturated O VI lines at each component velocity. The models also predict large O VII and O VIII column densities but suggest that the UV absorbers cannot account for all of the X-ray absorption detected in recent *Chandra* spectra. Finally, there is no evidence for a correlation between the characteristics of the UV absorbers and the UV continuum flux, and, by inference, the ionizing continuum. Hence, we suggest that the variations observed in the GHRS and STIS spectra are due

in a large part to changes in the column densities of the absorbers as the result of transverse motion.

Subject headings: galaxies: Seyfert - X-rays: galaxies - ultraviolet: galaxies - galaxies: individual (NGC 3783)

1.   Introduction

Since the launch of the *International Ultraviolet Absorber (IUE)*, it has been known that the UV spectra of Seyfert 1 galaxies show absorption lines intrinsic to their nuclei (Ulrich 1988). With the advent of the *HST*, it is now understood that intrinsic absorption is a common phenomenon, present in more than half of the well-studied Seyfert 1 galaxies (Crenshaw et al. 1999). Among those Seyferts that show absorption, high ionization lines such as N V $\lambda\lambda$1238.8, 1242.8 and C IV $\lambda\lambda$1548.2, 1550.8 are always present, along with Lyα, while lower ionization lines, such as Si IV $\lambda\lambda$1393.8, 1402.8 and Mg II $\lambda\lambda$2796.3, 2803.5, are less common. The absorption lines are blueshifted (by up to 2100 km s^{-1}) with respect to the systemic velocities of the host galaxies, indicating net radial outflow. The ionic columns are highly variable, which may be the result of changes in response to the ionizing continuum (cf. Krolik & Kriss 1997; Shields & Hamann 1997) or transverse motion (Crenshaw & Kraemer 1999). In either case, the variability is indicative of the promixity of the absorbers to the central active nucleus of these galaxies.

The presence of intrinsic absorption, typically in the form of bound-free edges of O VII and O VIII, has been detected in the X-ray spectra of a similar fraction of Seyfert 1 galaxies (Reynolds 1997; George et al. 1998). Most recently, spectra obtained with the *Chandra X-ray Observatory* have revealed that X-ray absorption lines associated with this material are also blue-shifted (Kaastra et al. 2000; Kaspi et al. 2000, hereafter K2000). The connection between the X-ray and UV absorption is complex. It has been argued that some fraction of the UV absorption arises in the same gas responsible for the X-ray absorption (Mathur, Elvis & Wilkes 1995, 1999; Crenshaw & Kraemer 1999; Kriss et al. 2000). Some sources, notably NGC 4151 (Kriss 1998; Kraemer et al. 2001) and NGC 3516 (Kriss et al. 1996; Crenshaw, Maran, & Mushotzky 1998) possess low ionization lines, indicative of a wide range in physical conditions within the absorbers. Furthermore, there is evidence that

the X-ray absorbers in some sources must also be multi-zoned (Otani et al. 1996; Reynolds et al. 1997).

NGC 3783 ($z = 0.00976$) is a bright, well-studied Seyfert 1 galaxy. During an *IUE* monitoring campaign from 1991 Decemeber 21 to 1992 July 29, the UV continuum showed rapid (20 – 40 days), large amplitude (factors of ~ 2 at 1460 Å) flux variations (Reichert et al. 1994). Intrinsic Lyα and C IV absorption were first detected in Faint Object Spectrograph (FOS) spectra by Reichert et al. (1994), and N V absorption was first seen in GHRS spectra by Lu, Savage, & Sembach (1994). Subsequent GHRS spectra revealed the UV absorption lines to be highly variable (Maran et al. 1996; Crenshaw 1999), with the C IV line becoming undetectable at one point (during observations taken in 1993 February 5). Observations with *ASCA* revealed the presence of a large ($> 10^{22}$ cm^{-2}) and variable column of ionized gas (George et al. 1998). Using photoionization models, with parameters derived from the fit to the X-ray absorber by George, Turner, & Netzer (1995), Shields & Hamann (1997) suggested that was plausible that the X-ray and UV absorption arose in a single zone, and that the changes in the absorber were due to the variable luminosity of the ionizing continuum. From spectra obtained with the High Energy Transmission Grating Spectrometer aboard *Chandra*, K2000 derived a mean velocity for the X-ray lines of $\approx 440 \pm 200$ km s^{-1}, which is consistent with the strong UV absorber discussed by Maran et al. (1996). Although this seems to support the suggestion that the absorbers are associated, the ionization state of the X-ray absorber observed by K2000 appears to be too high to produce the observed UV lines (although this depends on the spectral energy distribution [SED] of the ionizing radiation emitted by the central source). Interestingly, the total column of O VII K2000 derived from photoionization modeling of the absorption line gas is roughly an order of magnitude less than estimated using *ASCA* data (Reynold et al. 1997; George et al. 1998). Hence, the exact nature of the absorption in NGC 3783 is, as yet, undetermined.

NGC 3783 is one of the targets, along with NGC 5548 (Crenshaw & Kraemer 1999), NGC 4151 (Crenshaw et al. 2000; Kraemer et al. 2001) and NGC 3516 (Crenshaw & Kraemer, in preparation), in STIS Instrument Definition Team programs to investigate intrinsic absorption in Seyfert galaxies using medium resolution echelle spectra. In this paper, we present our analysis of the intrinsic absorber in NGC 3783, based on the echelle spectra and photoionization models. The paper is organized as follows: in Section 2 we describe the observations, in Section 3, we give the details of the measurement of the intrinsic lines, in Sections 4 and 5 we detail the photoionization modeling of the absorbers, and in Section 6 we discuss the implications of the results.

2. Observations

We obtained STIS medium-resolution echelle spectra of the nucleus of NGC 3783 through a $0''.2$ x $0''.2$ aperture on 2000 February 27. These observations, along with previous observations of the N V and C IV regions with the GHRS, are described in Table 1. The reduction of the GHRS spectra are described in Maran et al. (1996) and Crenshaw et al. (1999). We reduced the STIS echelle spectra using the IDL software developed at NASA's Goddard Space Flight Center for the STIS Instrument Definition Team. The data reduction includes a procedure to remove the background light from each order using a scattered light model devised by Lindler (1999). The individual orders in each echelle spectrum were spliced together in the regions of overlap.

Figure 1 shows a comparison of the GHRS and STIS spectra in the C IV region. As noted in Crenshaw et al. (1999), NGC 3783 shows dramatic variability in the column densities of the intrinsic C IV absorption lines. The GHRS spectrum on 1993 February 5 shows only Galactic C IV and C I lines (see Lu et al. 1994, Maran et al. 1996), and no evidence for intrinsic C IV absorption. However, 11 months later a C IV $\lambda\lambda1548.2$,

1550.8 doublet (component 2) appears at a radial velocity of -548 km s^{-1} (relative to the systemic redshift of z = 0.00976). After a subsequent interval of 15 months, another doublet (component 1) appears at -1365 km s^{-1}, and the original doublet is still present at about the same strength. Interestingly, just 16 days after no C IV absorption was detected in 1993, a GHRS spectrum shows the N V $\lambda\lambda1238.8$, 1242.8 doublet in absorption at the radial velocity of component 2.

Our STIS observations, obtained almost five years after the last GHRS spectrum, show more changes in the C IV absorption. The column density of component 1 has increased tremendously and a third C IV doublet has appeared at -724 km s^{-1}. This component (3) is very strong and blended with the others, so that careful deblending is required to determine the column densities of the individual components. [3]

Figure 2 shows the regions in the STIS E140M spectra where intrinsic absorption lines were detected (Lα, N V, C IV, and Si IV). Fluxes are plotted as a function of the radial velocity of the strongest member of each doublet, relative to the systemic redshift. Each of the three absorption components are present in Lα and the doublets of C IV and N V. Although it is difficult to distinguish component 2 in N V and C IV due to blending with component 3, its presence in Lα shows that this component has not disappeared at this epoch. Only component 1 is present in Si IV $\lambda\lambda1393.8$, 1402.8, indicating the presence of lower ionization gas in this component. Examination of the E230M spectrum reveals no discernable intrinsic absorption for any ion in this spectrum, including Mg II.

---

[3]The numbering of components is not intuitive. Crenshaw et al. (1999) numbered the first two components in order of increasing wavelength; however component 3 has now appeared in between these two.

3. Measurements

The procedures we used to measure the intrinsic absorption lines follow those of Crenshaw et al. (1999). To determine the shape of the underlying emission, we fit a cubic spline to regions on either side of the absorption. To normalize the absorption profiles, we divided the observed spectra by the spline fits. We consider the case where an absorber does not completely cover the emission sources behind it. If this effect is present and not corrected for, the column densities will be underestimated. We must therefore determine the covering factor C_{los}, which is the fraction of continuum plus BLR emission that is occulted by the absorber in our line of sight. We consider the case where the covering factor differs from one kinematic component to the next, but not within a component, as the signal-to-noise is not sufficient to determine the covering factor across the profiles. The value of C_{los} for a component can be determined from a doublet (Hamann et al. 1997). If the expected ratio of the optical depths of the doublet lines is 2 (as for C IV, N V, and Si IV), then

$$C_{los} = \frac{I_1^2 - 2I_1 + 1}{I_2 - 2I_1 + 1}, \tag{1}$$

where I_1 and I_2 are the residual fluxes in the cores of the weaker line (e.g., N V λ1242.8) and stronger line (e.g., N V λ1238.8), respectively.

As can be seen in Figure 2, the N V components are easier to isolate than those in C IV, and we therefore used the N V doublet to determine C_{los}. Table 2 gives C_{los} for each kinematic component, along with the radial velocity centroid and FWHM derived from the isolated components (see below). The covering factors for all three components are close to 0.6. By contrast, four other Seyfert 1 galaxies observed at high dispersion by *HST* have at least one component with $C_{los} > 0.9$ (Crenshaw et al. 1999).

Since the absorption components are resolved, we can determine the column density

of each component from its optical depth as a function of radial velocity (v_r). The optical depth at a particular radial velocity is:

$$\tau = ln\left(\frac{C_{los}}{I_r + C_{los} - 1}\right) \tag{2}$$

(Hamann et al. 1997).

The ionic column density is then obtained by integrating the optical depth across the profile:

$$N = \frac{m_e c}{\pi e^2 f \lambda} \int \tau(v_r) dv_r, \tag{3}$$

(Savage & Sembach 1991), where f is the oscillator strength and λ is the laboratory wavelength (Morton et al. 1988).

The kinematic components are blended in many cases, and we therefore used the following procedure to deblend the components and determine their ionic column densities. Since the absorption components are additive in optical depth, we converted the normalized absorption for each ion to optical depth (equation 2) as a function of radial velocity. For C IV, we derived the optical depth profile for component 1 directly from the λ1548.2 line in the STIS data (Figure 1). For C IV component 2, we used the combined λ1550.8 profile from the 1994 and 1995 GHRS observations, which is also unaffected by contaminating intrinsic or Galactic absorption. To obtain the profile for C IV component 3, we subtracted the component 1 doublet from the optical depth blend in the STIS data (given the 2:1 for the doublet). The profile for component 2 was obtained at a different time, so we scaled and subtracted the component 2 doublet until a reasonably smooth profile was obtained for component 3. With the optical depth profiles for each component, we then repeated the deblending process for the GHRS data until only the Galactic C I lines remained in this region.

For the N V components, we used a similar scheme. We obtained the optical depth profile of component 1 directly from the N V λ1238.8 line in the STIS data, and component

2 from the same line in the 1993 GHRS observation (see Crenshaw et al. 1999). The profiles of components 1 and 2 were then reproduced at the positions of the doublets in the STIS data, and scaled and subtracted until a smooth profile was obtained for component 3. The Si IV lines for component 1 are unaffected by contaminants, so we determined the optical depth profile directly from the STIS data. Errors in the optical depths were determined from the photon noise (which dominated in Si IV) and the uncertainties in scale factors used in the deblending process (which dominated in C IV and N V). For each kinematic component, the optical depth profiles for different ions as a function of radial velocity agree well; there is no evidence for a changing ionic ratio across any component. The small residuals obtained from the deblending process validate our assumption that the covering factors derived from N V are approximately correct for C IV and Si IV.

Table 2 gives the radial velocity centroids, widths (FWHM), and associated one-sigma errors for each kinematic component. These values represent the means and standard deviations determined from the measurements of the C IV and N V optical depth profiles (and the Si IV profile for component 3). As in previous studies (Crenshaw et al. 1999), we find no evidence for changes in velocity centroids or widths over time. In Table 3, we give the ionic column densities for each component, which were derived from the integration of optical depths according to equation 3. The Lyα absorption in each component appears to be heavily saturated, given the evidence for covering factors substantially smaller than one; we quote only lower limits for the H I in these components, derived from the $C_{los} = 1$ case. We have also determined upper limits to the columns of C II, Si II, and Mg II, which are given in Table 3.

4.   Inputs to the Photoionization Models

Photoionization models for this study were generated using the code CLOUDY90 (Ferland et al. 1998). We have modeled the absorbers as matter-bounded slabs of atomic gas, irradiated by the ionizing continuum radiation emitted by the central source. As per convention, the models are parameterized in terms of the ionization parameter, U, the ratio of the density of photons with energies $\geq$ 13.6 eV to the number density of hydrogen atoms at the illuminated face of the slab. Each separate kinematic component was initially modeled with one set of initial conditions, i.e., U, n_H, and the total hydrogen column density, N_H ($= N_{H\,I} + N_{H\,II}$)[4]. As discussed in Section 5, a second model (or "zone") was required to fit Component 1. For the models, we have assumed only thermal broadening, since 1) the absorption line widths could be due to the superposition of unresolved kinematic components and 2) comparison models assuming turbulent velocities of $\leq$ 300 km s^{-1} predicted nearly identical ionic columns. As in similar studies (e.g. Crenshaw & Kraemer 1999), a model is deemed successful when the predicted ionic column densities, specifically those of N V, C IV and (in one case) Si IV, provide a good match (i.e., better than a factor of 2) to those observed in the STIS spectra.

In order to approximate the SED of the ionizing continuum, we assumed it to be a power-law of the form $F_\nu \propto \nu^{-\alpha}$. Based on *ASCA* observations, George et al. (1998) fit the 0.6 – 10 keV with a power-law of index $\alpha \approx 0.8$, with an average flux in the 0.1 - 10 keV band of $\sim$ 2.8 x 10^{-10} ergs s^{-1} cm^{-2} (which yields $F_\nu \sim$ 3.5 x 10^{-28} ergs s^{-1} cm^{-2} Hz^{-1} at 0.6 keV). In our STIS spectra, the flux at 1470 Å is $F_\nu \approx$ 2.53 x 10^{-26} ergs s^{-1} cm^{-2} Hz^{-1}. In order to determine the flux at the Lyman limit, we extrapolated to 912 Å assuming a power-law with a spectral index of $\alpha = 1$, which yields a flux of $F_\nu \sim$ 7.5 x 10^{-26} ergs s^{-1}

---

[4]We use N(XM) to denote the ionic column density, where "X" is the atomic symbol and "M" is the ionization state.

cm^{-2} Hz^{-1}, after correcting for reddening (E$_{B-V}$ = 0.12; Reichert et al. 1994). Extending the X-ray continuum to UV wavelengths underpredicts the observed UV flux by more than two orders of magnitude and, therefore, the continuum must steepen at energies below 0.6 keV. For the sake of simplicity, we assumed that the break in the continuum occurs at this energy. Therefore, we assume the following UV to X-ray spectral indices: $\alpha = 1$ below 13.6 eV, $\alpha = 1.4$ over the range 13.6 eV $\leq h\nu < 600$ eV, and $\alpha = 0.8$ above 600 eV. It should be noted that the power-law break could occur at lower energies and/or that a "Big Blue Bump" may be present (see George et al. 1995). If the former were the case, the relative fractions of highly ionized species, such as O VII and O VIII, would be somewhat higher than our predictions, while in the latter case the opposite would be true. The lack of simultaneous UV and X-ray observations introduces an additional uncertainty in modeling the SED.

We have assumed roughly solar element abundances (cf. Grevesse & Anders 1989), which are, by number relative to H, as follows: He = 0.1, C = 3.4 x 10^{-4}, N = 1.2 x 10^{-4}, O = 6.8 x 10^{-4}, Ne = 1.1 x 10^{-4}, Mg = 3.3 x 10^{-5}, Si = 3.1 x 10^{-5}, S = 1.5 x 10^{-5}, and Fe = 4.0 x 10^{-5}. The absorbing gas is assumed to be free of cosmic dust.

5.   Model Results

Component 1, the most blueshifted of the absorbers, is the only one to possess detectable Si IV absorption. The ratio of N(N V)/N(C IV) is > 2, which is indicative of highly ionized gas (see, for example, Shields & Hamann 1997), while, on the other hand, the fact that N(C IV)/N(Si IV) is smaller than the abundance ratio is evidence for much lower ionization gas. Based on our experience modeling the absorbers in NGC 4151 (Kraemer et al. 2001), this dilemma can be resolved if the ionizing continuum were modified by an intervening absorber which is optically thick from 13.6 eV – 100 eV, however there is

no evidence for such material in our line-of-sight to the nucleus of NGC 3783. A simpler explanation is that Component 1 consists of two zones characterized by different ionization parameters, with similar covering factors and velocity profiles; in this scenario, the lower ionization absorption could arise in gas co-located with the more tenuous, and thus more highly ionized, absorber. We modeled Component 1 using two separate zones with the following parameters: 1) U= 0.78, N_H = 1.2 x 10^{21} cm^{-2}, and 2) U = 0.0018, N_H = 4.9 x 10^{18} cm^{-2}. The predicted ionic columns are listed in Tables 4 and 5, respectively (the ions used to constrain the models are shown in boldface). If the two zones are at the same radial distance, the density of the lower ionization zone is $\sim$ 430 times higher. The sums of the predicted ionic columns from the two zones provide a good fit to the observed columns. Also, the low ionization model predictions for N(C II) and N(Si II), are below their respective 2σ limits, which agrees with the non-detection of such lines in the STIS spectra. It should be noted that the models slightly underpredict N(Si IV) and overpredict N(C IV). [5]

Based on the ratio of the N V and C IV column densities ($\sim$ 5.8), Component 2 is the most highly ionized of the 3 kinematic components detected in the STIS spectra. As shown in Table 6, we were able to fit the observed ionic columns with a single-zoned model, parameterized as follows: U = 0.80 and N_H = 6.4 x 10^{20} cm^{-2}. Nevertheless, due to the large uncertainties in the measured columns (see Table 3), the physical conditions in Component 2 are not tightly constrained. For example, if the N V to C IV ratio were $\sim$ 10

---

[5]The only way to increase N(Si IV), given the absence of lower ionization lines, is to increase both the ionization parameter and column density of the low ionization zone model. However, even slight changes ($\sim$ 20%) in these parameters would worsen the N(C IV) prediction. We will be better able constrain the range in physical conditions in Component 1 with the series of observations taken during our monitoring campaign (see Section 7).

(which is well within the errors), the ionization parameter would be ~ 2.0 and $N_H \sim 10^{22}$ cm^{-2}, which would yield an order of magnitude increase in O VII and O VIII columns.

While Component 3 possesses the strongest N V absorption, the N(N V)/N(C IV) ratio is less than that of Component 2, indicative of a lower ionization parameter. As shown in Table 7, we were able to match the observed column densities with a single-zoned model parameterized as follows: $U = 0.65$ and $N_H = 1.5 \times 10^{21}$ cm^{-2}.

In summary, we have been able to fit the measured ionic column densities with simple one- or two-zoned photoionization models. There is no evidence for anomalous abundances or cosmic dust (i.e., depletions of elements from gas phase) within the absorbers. None of the absorbers possesses sufficient opacity at the H I or He II Lyman limits to affect the ionization state of gas further from the nucleus (for a discussion of this effect, see Kraemer et al. 1999), hence we see no effects due to the screening of one absorbing component by another.

6. Discussion

6.1. X-ray and far-UV Absorption

Based on our model predictions, all three components should possess substantial columns of O VII, and O VIII. The summed O VII and O VIII columns are 1.3×10^{18} cm^{-2} and 7.7×10^{17} cm^{-2}, respectively. The predicted O VIII column is 5 times less than that determined by K2000, based on modeling of roughly contemporary *Chandra* spectra, while the predicted O VII column is a factor of 2.6 greater. Although the predicted and observed column densities do not agree, the radial velocities of Components 2 and 3 are roughly consistent with the mean value of the X-ray absorption lines (K2000). If the Component 2 is more highly ionized than indicated by the mean N V to C IV ratio, its O VIII column

may be significantly larger. However, this would worsen the fit for O VII and the model would still underpredict the columns of the high ionization species detected by K2000, such as Si XIV, Fe XVIII, and Fe XIX. Since the N V and C IV columns in Component 3 have much smaller errors, the ionization parameter is well constrained by the models, hence the absorber cannot produce the observed O VIII column. Interestingly, our model for Component 1 predicts an O VII $\lambda 18.6$ line with an $EW = 26$ mÅ and O VIII $\lambda 16.0$ line with an $EW = 28$ mÅ . Although not reported by K2000, perhaps these feature are present on the blue wings of the lines detected in the *Chandra* spectra.

To summarize, although slight variations in our model parameters could bring the O VII prediction into agreement with the *Chandra* results, a substantial fraction of the X-ray absorbing gas is too highly ionized to produce UV absorption. Also, the O VII column reported by K2000 is significantly less than that determined from previous *ASCA* results (Reynolds 1997; George et al. 1998) which implies that the either 1) the absorbing column was larger in the past, or 2) there are unknown problems in determining the O VII column from one of these datasets. In either case, we cannot, with sufficient certainty, establish a one-to-one connection between the X-ray and UV absorbers.

In Table 8 we list the line center optical depths, based on our model predictions, for several far-UV lines which will be detectable with *FUSE*. Clearly, the O VI $\lambda\lambda 1031.9, 1037.6$ lines will be saturated ($\tau_{center} > 4$) for all three kinematic components, and Component 1 should possess saturated C III $\lambda 997$ and strong N III $\lambda 990$. Although, as noted in Section 2, Lyα is saturated in each component, our results indicate that Lyβ and Lyγ may not be in Components 2 and 3. Hence these lines could be used to determine the total H I column, which, in turn, can be used to test our model assumptions (and better constrain the physical conditions in Component 2).

6.2. Changes in the UV Absorbers

Although the column densities of the UV absorbers in NGC 3783 (and other Seyfert 1s) are known to change over time (see Crenshaw et al. 1999), these variations could be due to the response of the absorbers to changes in the ionizing flux, changes in total column due to transverse motion, or some combination of these effects. In NGC 4151, Kraemer et al. (2001) argued that the largest changes in the UV absorbers were well-correlated with changes in the ionizing continuum, while for NGC 5548, Crenhsaw & Kraemer (1999) found that transverse motion was a more plausible explanation. Shields & Hamann (1997) suggested that the variations in UV absorption observed in NGC 3783 are a function of changes in the luminosity of the ionizing source. Here, we re-examine this suggestion, using an additional GHRS observation (from 1995 April 11) along with our STIS dataset (we have not included the FOS data from 1992 July 27 in this analysis, due to the unreliability of ionic column density measured in low resolution spectra).

Figure 3 shows the changes in the the C IV columns, assuming that undetectable columns are $< 3 \times 10^{13}$ cm^{-2}, and the UV continuum over time. First, the C IV columns do not seem to be correlated with the UV flux. For Component 2, the C IV is undetectable in 1993 and strong in 1994, during which time the continuum flux decreases, and the column decreases from 1995 to 2000 while the flux increases. Although these column changes could be interpreted as a response to the continuum flux, this cannot also explain the the weak response between 1994 and 1995, during which time the UV flux has dropped sharply. Furthermore, Component 3 would have to be undetectable at both low and high ionization states to have missed detection in earlier epochs. Given our two-zone model for Component 1, it is difficult to produce the increase in the C IV column from 1995 to the present solely by increasing the ionizing flux, since most of the gas is in the high ionization zone. We have also determined the ionization parameters that describe the physical state of the absorbers

at each epoch, assuming that N_H is constant (i.e., no transverse motion). As shown in Figure 3, the variations are not correlated with the changes in the UV flux. For example, there is no evidence that U is at a mininum for any of the three components during 1995, when the UV flux was weakest. Based on this, we see no evidence that the state of the UV absorbers is simply the result of changes in the ionizing flux.

Alternatively, much of the observed variations in UV ionic columns could be explained by transverse motion. For example, assuming constant U, the different C IV columns observed in Component 2 correspond to values of N_H ranging from 3.2 x 10^{20} cm^{-2} (in 1993) to 1.5 x 10^{21} cm^{-2} (in 1994). The predicted C IV column in 1993 would be 3.0 x 10^{13} cm^{-2}, which is at the detectability limit and could explain the absence of a noticeable feature. For Component 1, the smaller C IV column observed in 1995 could be simply due to the absence of the low ionization zone. Similarly, the absence of Component 1 in earlier epochs could be the result of a smaller column of the high ionization gas, as may be the case for Component 3.

Although the changes in the ionic columns could be due solely to transverse motion, we cannot rule out a combination of a changes in both total column density and ionization state. Deconvolving these effects requires an intensive monitoring program, rather than the poor sampling provided by the few available observations. Unfortunately, if the variations are primarily due to transverse motion, one cannot rely on recombination/ionization timescales to constrain the densities of the absorbers.

7.   Summary

We have used medium resolution echelle spectra obtained with *HST*/STIS to study the physical conditions in the intrinsic UV absorbers in the Seyfert 1, NGC 3783 and have

determined the following.

1. The appearance of the UV absorption has changed noticeably since the most recent GHRS observations (taken in 1995). There are currently three distinct kinematic components, at velocities of -1365, -548, and -724 km s^{-1}, with respect to the systemic velocity of the host galaxy. Each component possesses C IV $\lambda\lambda$1548.2, 1550.8, N V $\lambda\lambda$1238.8, 1242.8, and heavily saturated Lyα lines, while Component 1 also shows the presence of Si IV $\lambda\lambda$1393.8, 1402.8. Component 3, which has the largest N V column density, was absent in all earlier observations. As shown in Table 2, each component has a covering factor of less than unity. The simplest explanation is that the absorbers do not cover the entire broad line region, but other geometries cannot be ruled out. In order to constrain the ionization state and total hydrogen column densities of the absorbers, we used photoionization models predictions to match the measured ionic column densities. Components 2 and 3 were well matched by single zoned models, while it required two zones of different ionization parameter to fit Component 1. The ionization parameters and hydrogen column densities were somewhat higher than those observed in NGC 5548, with the exception of the one component in that galaxy which may be associated with the X-ray absorption (Crenshaw & Kraemer 1999).

2. In contrast with Shields & Hamann (1997), we do not find strong evidence that the changes in the UV absorption are a function of variations in the ionizing continuum. In fact, we find that these variations may be more readily explained by transverse motion, which results in changes the total column of gas along our line-of-sight. Nevertheless, it is possible that both continuum variations and transverse motion contribute to the variability of the absorption.

3. We predict that far-UV, *FUSE* spectra will show O VI $\lambda\lambda$1031.9, 1037.6 absorption lines at the velocities of the each UV kinematic component, and C III λ977 and N III λ990

at the velocity of Component 1. The higher order Lyman lines will not be saturated for Components 2 and 3, and, hence can be used to check our model predictions. Although the photoionization models predict substantial O VII and O VIII columns, and there is an apparent coincidence between the velocity of UV Component 2 and the mean velocity of the X-ray absorption lines, the absorbing gas is at a lower ionization state and of smaller total column than the gas responsible for the much of the X-ray absorption seen in *ASCA* (Reynolds 1997; George et al 1998) and *Chandra* (K2000) spectra. Hence, it is likely that the X-ray absorber consists of two of more zones, characterized by different physical conditions. The determination of the detailed relationship between the UV and X-ray absorption, and the nature of their variability, will require simultaneous observations and better sampling, which are the principal goals of an *HST*, *FUSE*, and *Chandra* monitoring campaign.

REFERENCES

Crenshaw, D.M., Maran, S.P, & Mushotzky, R.F. 1998, ApJ, 496, 797

Crenshaw, D.M., & Kraemer, S.B. 1999, ApJ, 521, 572

Crenshaw, D.M., Kraemer, S.B., Boggess, A., Maran, S.P., Mushotzky, R.F., & Wu, C.-C. 1999, ApJ, 516, 750

Ferland, G.J. et al. 1998, PASP, 110, 761

Crenshaw, D.M., et al. 2000, ApJ, 545, L27

George, I.M., Turner, T.J., & Netzer, H. 1995, ApJ, 438, L67

George, I.M., Turner, T.J., Netzer, H., Nandra, K., Mushotzky, R.F., & Yaqoob, T. 1998a, ApJS, 114, 73

Grevesse, N., & Anders, E. 1989, in Cosmic Abundances of Matter, ed. C.J. Waddington (New York: AIP), 1

Hamann, F., Barlow, T.A., Junkkarinen, V., & Burbidge, E. M. 1997, ApJ, 478, 78

Kaastra, J.S., Mewe, R., Liedahl, D.A., Komossa, S., & Brinkman, A.C. 2000, A&A, 354, L83

Kaspi, S., Brandt, W.N., Netzer, H., Sambruna, R., Chartas, G., Garmire, G.P., & Nousek, J.A. 2000, ApJ, 535, L17 (K2000)

Kraemer, S.B., et al. 2001, ApJ, in press

Kriss, G.A. 1998, in The Scientific Impact of the Goddard High Resolution spectrograph, ed. J.C. Brandt, T.B. Ake, & C.C. Petersen (San Francisco: Astronomical Society of the Pacific), ASP Conference Series, 143, 271

Kriss, G.A., Espey, B.R., Krolik, J.H, Tsvetanov, Z., Zheng, W., & Davidsen, A.F. 1996, ApJ, 467, 222

Kriss, G.A., et al. 2000, ApJ, 538, L17

Krolik, J.H., & Kriss, G.A. 1997, in Mass Ejection from Active Galactic Nuclei, ed. N. Arav, I. Shlosmann, & R.J. Weymann (San Francisco: Astronomical Society of the Pacific), ASP Conference Series, 128, 132

Lindler, D. 1998, CALSTIS Reference Guide (CALSTIS Version 5.1)

Lu, L., Savage, B.D., & Sembach, K.R. 1994, ApJ, 426, 563

Maran, S.P., et al. 1996, ApJ, 465, 733

Mathur, S., Elvis, M., & Wilkes, B.J. 1999, ApJ, 519, 605

Mathur, S., Elvis, M., & Wilkes, B.J. 1995, ApJ, 452, 230

Morton, D.C., York, D.G., & Jenkins, E.B. 1988, ApJS, 68, 449

Otani, C., et al. 1996, PASP, 48, 211

Reichert, G.A., et al. 1994, ApJ, 425, 582

Reynolds, C.S. 1997, MNRAS, 286, 513

Reynolds, C.S., Ward, M.J, Fabian, A.C., & Celotti, A. 1997, MNRAS, 286, 513

Savage, B.D., & Mathis, J.S. 1979, ARA&A, 17, 73

Savage, B.D., & Sembach, K.R. 1991, ApJ, 379, 245

Shields, J.C., & Hamann, F. 1997, ApJ, 481, 752

Ulriich, M.-H. 1988, MNRAS, 230, 121

Fig. 1.— GHRS and STIS spectra of the C IV region in NGC 3783. The Galactic lines are labeled in the top spectrum, and are due primarily to C IV $\lambda\lambda$1548.2, 1550.8 and C I λ1560.3 near the local standard of rest and C I λ1560.3 from a Galactic high-velocity cloud at +240 km s^{-1} (Lu et al. 1993; Maran et al. 1996). The kinematic components of the intrinsic C IV absorption doublets are numbered. Dotted lines show the zero flux levels.

Fig. 2.— Portions of the STIS echelle spectra of NGC 3783, showing the intrinsic absorption lines detected. Fluxes are plotted as a function of the radial velocity (of the strongest member, for the doublets), relative to an emission-line redshift of z = 0.00976. The kinematic components are identified with large and small numbers, for the strong and weak members of the doublets respectively. Absorption lines that are not labeled are Galactic. The "broad absorption" feature seen in the Si IV profile near +2800 km s^{-1} is an artifact due to the STIS FUV MAMA repeller wire.

Fig. 3.— Continuum and C IV absorption variations in *HST* high-resolution spectra as a function of Julian date. The top plot shows the continuum variations at 1470 Å in units of 10^{-14} ergs s^{-1} cm^{-2} Å^{-1}. The middle plot show variations in the C IV column density (Table 3) in units of 10^{14} cm^{-2} for each component (1, 2, and 3). The lower plots shows ionization parameters (U) derived from photoionization models assuming constant hydrogen column density, as described in the text.

Table 1.   *HST* High-Resolution Spectra of NGC 3783

Instrument	Grating	Coverage (Å)	Resolution ($\lambda/\Delta\lambda$)	Exposure (sec)	Date (UT)
STIS	E140M	$1150 - 1730$	46,000	5400	2000 February 27
STIS	E230M	$2274 - 3119$	30,000	2191	2000 February 27
GHRS	G160M	$1527 - 1597^a$	20,000	4134^b	1993 February 5
GHRS	G160M	$1232 - 1269^c$	20,000	8064	1993 February 21
GHRS	G160M	$1527 - 1597^a$	20,000	4788^b	1994 January 16
GHRS	G160M	$1527 - 1597^a$	20,000	4352^b	1995 April 11

[a]Includes the C IV region (Maran et al. 1996; Crenshaw et al. 1999).

[b]per grating setting; two settings were used.

[c]Includes the N V region (Lu et al. 1994; Crenshaw et al. 1999.)

Table 2.   Absorption Components in NGC 3783

Component	Velocity[a]	FWHM	C_{los}[b]
	(km s^{-1})	(km s^{-1})	
1	$-1365\ (\pm 20)$	193 (± 17)	0.61 (± 0.04)
2	$-548\ (\pm 15)$	170 (± 13)	0.60 (± 0.05)
3	$-724\ (\pm 15)$	280 (± 30)	0.65 (± 0.03)

[a]Velocity centroid for a systemic redshift of z = 0.00976.

[b]Covering factor in the line of sight from the N V doublet.

Table 3.   Ionic Column Densities $(10^{14}\ \mathrm{cm}^{-2})^a$

Date (UT)	Ion	Component 1	Component 2	Component 3
1993 Feb. 5, 21	C IV	——	——	——
	N V	——	1.84 ($\pm$0.19)	——
1994 Jan. 16	C IV	——	1.48 ($\pm$0.29)	——
1995 Apr. 11	C IV	2.09 ($\pm$0.34)	1.24 ($\pm$0.23)	——
2000 Feb. 27	C IV	3.50 ($\pm$0.34)	0.63 ($\pm$0.24)	3.23 ($\pm$0.48)
	N V	7.60 ($\pm$1.50)	3.68 ($\pm$1.84)	16.03 ($\pm$2.32)
	Si IV	0.61 ($\pm$0.19)	——	——
	H I	> 0.84	>0.77	>3.86
	C II	<1.0	<1.0	<1.0
	Si II	<0.3	<0.3	<0.3
	Mg II	<0.1	<0.1	<0.1

[a]quoted errors are 1σ values.

Table 8.　Predicted Line Center Optical Depths for far-UV lines

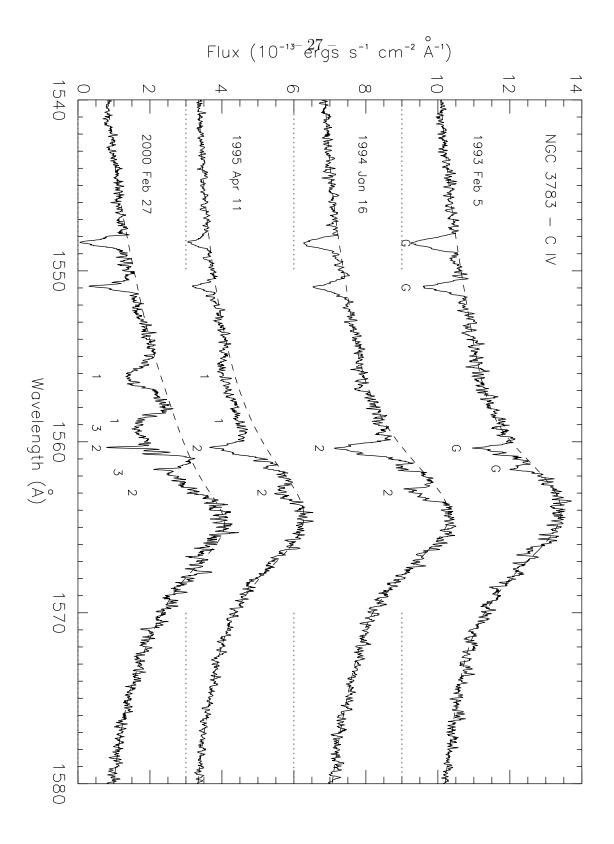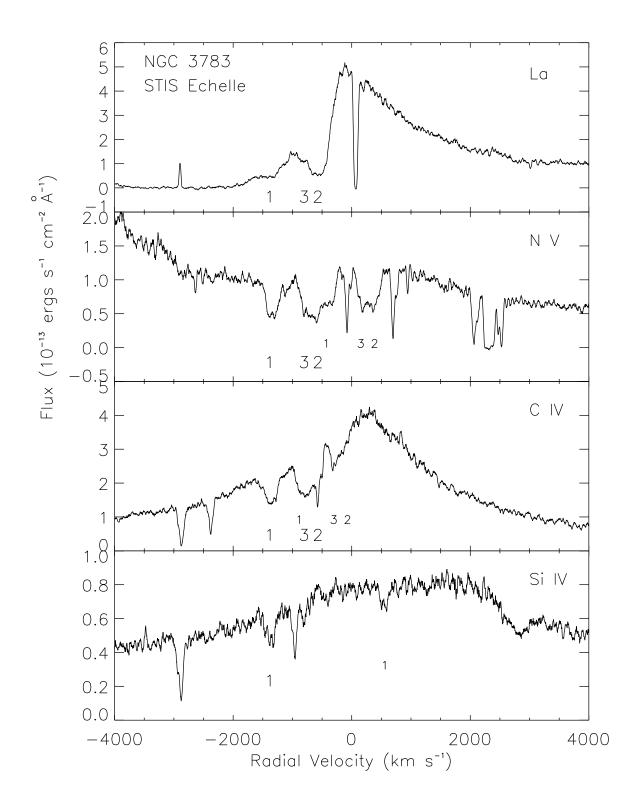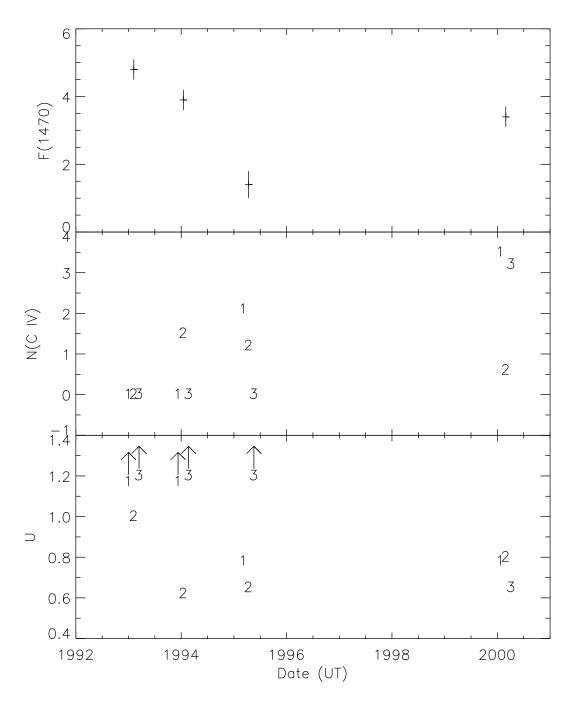| Ion	Line	N (cm^{-2})	τ_{center}
	Component 1	(FWHM = 193 km s^{-1})	
H I	Lyα	2.0 x 10^{16}	130
	Lyβ		21
	Lyγ		7
C III	λ977	1.2 x 10^{15}	11
N III	λ990	4.2 x 10^{14}	0.57
O VII	λ1032	2.6 x 10^{16}	44
	Component 2	(FWHM = 170 km s^{-1})	
H I	Lyα	1.7 x 10^{15}	13
	Lyβ		2.0
	Lyγ		0.7
O VII	λ1032	1.3 x 10^{16}	25
	Component 3	(FWHM = 280 km s^{-1})	
H I	Lyα	5.5 x 10^{15}	25
	Lyβ		4
	Lyγ		1.4
O VII	λ1032	4.9.3 x 10^{16}	58

Fig. 1.

Fig. 2.

Fig. 3.

TABLE 4

Component 1 (High Ionization): Predicted Ionic Column Densities[a] (in units of cm^{-2}

Element	I XI	II XII	III XIII	IV XIV	V XV	VI XVI	VII XVII	VIII XVIII	IX XIX
H	3.3×10^{15}	1.2×10^{21}							
He	–	5.3×10^{16}	1.2×10^{20}						
C	–	–	–	$\mathbf{1.3 \times 10^{14}}$	3.7×10^{16}	2.0×10^{17}	1.7×10^{17}		
N	–	–	–	2.6×10^{13}	$\mathbf{7.6 \times 10^{14}}$	4.5×10^{16}	7.4×10^{16}	2.4×10^{16}	
O	–	–	–	6.8×10^{13}	2.5×10^{15}	2.6×10^{16}	4.5×10^{17}	3.0×10^{17}	4.5×10
Ne	–	–	–	–	2.6×10^{14}	7.2×10^{15}	1.5×10^{16}	2.7×10^{16}	7.1×10
	4.5×10^{14}								
Mg	–	–	–	–	–	–	2.3×10^{14}	3.3×10^{15}	1.3×10
	8.7×10^{15}	4.2×10^{14}	–						
Si	–	–	–	–	–	–	2.8×10^{13}	6.9×10^{14}	4.8×10
	1.4×10^{16}	4.3×10^{15}	1.2×10^{15}	2.2×10^{13}	–				
S	–	–	–	–	–	–	–	5.2×10^{13}	6.8×10
	6.4×10^{15}	5.4×10^{15}	1.9×10^{15}	3.0×10^{14}	4.5×10^{13}	–			
Fe	–	–	–	–	–	–	–	–	2.5×10
	1.3×10^{15}	5.3×10^{15}	1.1×10^{16}	1.2×10^{16}	1.1×10^{16}	3.7×10^{15}	2.7×10^{15}	3.2×10^{14}	2.4×10

[a]Model Parameters: U = 0.78, $\mathrm{N}_H = 1.2 \times 10^{21}$ cm^{-2}. The dash indicates a column $< 10^{13}$ cm^{-2}.

TABLE 5

CORRESPONDS TO: COMPONENT 1 (LOW IONIZATION): PREDICTED IONIC COLUMN DENSITIES[a] (IN UNITS OF CM^{-2})

| Element | I | II | III | IV | V | VI | VII | VIII | IX | X |
	XI	XII	XIII	XIV	XV	XVI	XVII	XVIII	XIX	XX
H	1.7×10^{16}	4.9×10^{18}								
He	8.9×10^{14}	1.7×10^{17}	3.2×10^{17}							
C	–	1.5×10^{14}	1.2×10^{15}	$\mathbf{2.9 \times 10^{14}}$	4.6×10^{13}	–	–			
N	–	3.6×10^{13}	4.2×10^{14}	1.2×10^{14}	–	–	–	–		
O	–	1.8×10^{14}	2.1×10^{15}	9.5×10^{14}	2.3×10^{15}	8.0×10^{13}	–	–	–	
Ne	–	1.2×10^{13}	3.7×10^{14}	1.4×10^{14}	1.5×10^{13}	–	–	–	–	–
	–									
Mg	–	–	1.1×10^{14}	4.1×10^{13}	–	–	–	–	–	–
	–	–	–							
Si	–	1.1×10^{13}	7.8×10^{13}	$\mathbf{4.1 \times 10^{13}}$	2.0×10^{13}	–	–	–	–	–
	–	–	–	–	–					
S	–	–	4.5×10^{13}	1.9×10^{13}	–	–	–	–	–	–
	–	–	–	–	–	–				
Fe	–	–	–	6.4×10^{13}	8.5×10^{13}	3.4×10^{13}	–	–	–	–
	–	–	–	–	–	–				

[a] Model Parameters: U = 0.0018, $N_H = 4.9 \times 10^{18}$ cm^{-2}. The dash indicates a column $< 10^{13}$ cm^{-2}.

TABLE 6

Component 2: Predicted Ionic Column Densities[a] (in units of cm^{-2})

Element	I / XI	II / XII	III / XIII	IV / XIV	V / XV	VI / XVI	VII / XVII	VIII / XVIII	IX / XIX
H	1.7×10^{15}	6.4×10^{20}							
He	–	2.7×10^{16}	6.4×10^{19}						
C	–	–	–	$\mathbf{6.2 \times 10^{13}}$	1.8×10^{16}	1.0×10^{17}	9.5×10^{16}		
N	–	–	–	1.2×10^{13}	$\mathbf{3.7 \times 10^{14}}$	2.3×10^{16}	4.0×10^{16}	1.4×10^{16}	
O	–	–	–	3.3×10^{13}	1.2×10^{15}	1.3×10^{16}	2.3×10^{17}	1.6×10^{17}	2.6×10
Ne	–	–	–	–	1.2×10^{14}	3.5×10^{15}	7.7×10^{15}	1.4×10^{16}	3.9×10
	2.7×10^{14}								
Mg	–	–	–	–	–	–	1.2×10^{14}	1.7×10^{15}	6.9×10
	4.8×10^{15}	2.5×10^{14}	–						
Si	–	–	–	–	–	–	1.3×10^{13}	3.4×10^{14}	2.5×10
	7.4×10^{15}	2.4×10^{15}	6.7×10^{14}	1.3×10^{13}	–				
S	–	–	–	–	–	–	–	2.3×10^{13}	3.2×10
	3.3×10^{15}	3.0×1015	1.1×10^{15}	1.8×10^{14}	2.8×10^{13}	–			
Fe	–	–	–	–	–	–	–	–	1.3×10
	6.2×10^{14}	2.6×10^{15}	5.7×10^{15}	6.4×10^{15}	6.0×10^{15}	2.0×10^{15}	1.6×10^{15}	2.0×10^{14}	1.5×10

[a]Model Parameters: U = 0.80, N$_H$ = 6.4×10^{20} cm^{-2}. The dash indicates a column < 10^{13} cm^{-2}.

TABLE 7

COMPONENT 3: PREDICTED IONIC COLUMN DENSITIES[a] (IN UNITS OF CM^{-2})

Element	I / XI	II / XII	III / XIII	IV / XIV	V / XV	VI / XVI	VII / XVII	VIII / XVIII	IX / XIX
H	5.5×10^{15}	1.5×10^{21}							
He	–	8.7×10^{16}	1.5×10^{20}						
C	–	–	–	$\mathbf{3.2 \times 10^{14}}$	6.6×10^{16}	2.7×10^{17}	1.7×10^{17}		
N	–	–	–	6.4×10^{13}	$\mathbf{1.6 \times 10^{15}}$	7.0×10^{16}	8.7×10^{16}	2.1×10^{16}	
O	–	–	–	1.5×10^{14}	5.4×10^{15}	4.9×10^{16}	6.2×10^{17}	3.1×10^{17}	3.5×10
Ne	–	–	–	–	6.8×10^{14}	1.5×10^{16}	2.6×10^{16}	3.8×10^{16}	7.6×10
	2.8×10^{14}								
Mg	–	–	–	–	–	1.1×10^{13}	4.1×10^{14}	4.8×10^{15}	1.9×10
	8.2×10^{15}	3.0×10^{14}	–						
Si	–	–	–	–	–	–	7.3×10^{13}	1.4×10^{15}	8.1×10
	1.5×10^{16}	3.9×10^{15}	8.5×10^{14}	1.2×10^{13}					
S	–	–	–	–	–	–	–	1.6×10^{14}	1.6×10
	8.2×10^{15}	5.2×1015	1.4×10^{15}	1.8×10^{14}	2.3×10^{13}	–			
Fe	–	–	–	–	–	–	–	1.7×10^{13}	4.9×10
	3.3×10^{15}	9.9×10^{15}	1.5×10^{16}	1.4×10^{16}	1.0×10^{16}	3.6×10^{15}	1.9×10^{15}	1.8×10^{14}	1.0×10

[a]Model Parameters: U = 0.65, N$_H$ = 1.5 x 10^{21} cm^{-2}. The dash indicates a column < 10^{13} cm^{-2}.